Exploring the Growth Index γ_L: Insights from Different CMB Dataset Combinations and Approaches

Enrico Specogna,[1,*] Eleonora Di Valentino,[1,†] Jackson Levi Said,[2,3,‡] and Nhat-Minh Nguyen[4,5,§]

[1] *School of Mathematics and Statistics, University of Sheffield, Hounsfield Road, Sheffield S3 7RH, United Kingdom*
[2] *Institute of Space Sciences and Astronomy, University of Malta*
[3] *Department of Physics, University of Malta*
[4] *Leinweber Center for Theoretical Physics, University of Michigan, 450 Church St, Ann Arbor, MI 48109-1040*
[5] *Department of Physics, College of Literature, Science and the Arts, University of Michigan, 450 Church St, Ann Arbor, MI 48109-1040*

arXiv:2305.16865v2 [astro-ph.CO] 2 Feb 2024

In this study we investigate the growth index γ_L, which characterizes the growth of linear matter perturbations, while analysing different cosmological datasets. We compare the approaches implemented by two different patches of the cosmological solver `CAMB`: `MGCAMB` [1–5] and `CAMB_GammaPrime_Growth` [6, 7]. In our analysis we uncover a deviation of the growth index from its expected ΛCDM value of 0.55 when utilizing the Planck dataset, both in the `MGCAMB` case and in the `CAMB_GammaPrime_Growth` case, but in opposite directions. This deviation is accompanied by a change in the direction of correlations with derived cosmological parameters. However, the incorporation of CMB lensing data helps reconcile γ_L with its ΛCDM value in both cases. Conversely, the alternative ground-based telescopes ACT and SPT consistently yield growth index values in agreement with $\gamma_L = 0.55$. We conclude that the presence of the $A_{\rm lens}$ problem in the Planck dataset contributes to the observed deviations, underscoring the importance of additional datasets in resolving these discrepancies.

I. INTRODUCTION

The standard model of cosmology embodies the most universally accepted concordance model for both astrophysical and cosmological regimes within an isotropic and homogeneous Universe [8, 9]. In this model, cold dark matter (CDM) acts as a stabilizing agent for galaxies and their clusters [10–12], while the late-time accelerating expansion of the Universe is sourced by a cosmological constant Λ [13, 14]. In this scenario, initial cosmic inflation drove the early Universe towards flatness that observes the cosmological principle [15, 16].

However, challenges persist within this framework. The cosmological constant continues to pose theoretical difficulties [17, 18], while the direct detection of CDM remains problematic [11, 12], and the UV completeness of the theory remains an open question [19]. In recent years, additional challenges to ΛCDM cosmology have emerged in the form of cosmic tensions. These tensions arise from discrepancies between direct measurements of the cosmic expansion rate and the growth of large scale structure (LSS), and those inferred indirectly from early Universe measurements [20–29].

The presence of cosmic tensions has become evident across multiple surveys, primarily manifested in the measurement of the Hubble constant, H_0, which has now exceeded 5σ [30–33]. The indirect measurements of H_0 mainly rely on observations of the Cosmic Microwave Background radiation (CMB) with the latest reported value by the Planck collaboration giving $H_0 = 67.4 \pm 0.5\,\mathrm{km\,s^{-1}Mpc^{-1}}$ [34], while the last release from ACT puts $H_0 = 67.9 \pm 1.5\,\mathrm{km\,s^{-1}Mpc^{-1}}$ [35]. Conversely, late time probes offer several alternatives for the direct measurement of the Hubble expansion of the Universe. Among these, the most precise measurements are based on Type Ia Supernovae (SNIa) by the SH0ES Team, calibrated by Cepheids, yielding $H_0 = 73.04 \pm 1.04\,\mathrm{km\,s^{-1}Mpc^{-1}}$ [36]. Numerous other measurements also consistently favor higher values for the Hubble constant [37–44]. Finally, the latest measurements employing the Tip of the Red Giant Branch as a calibration method for SNIa continue to indicate elevated values for H_0 [45–48].

Another cosmological tension that is gaining significance relates to the growth of large-scale structures in the Universe. Several parameters capture these characteristics, with $S_8 = \sigma_{8,0}\sqrt{\Omega_{\rm m,0}/0.3}$ being a key quantity that incorporates the matter density parameter at present $\Omega_{\rm m,0}$ and is commonly used to quantify it, as it is directly measured by Weak Lensing (WL) experiments. The measurement of S_8 is more challenging, with discrepancies between early- and late-time probes ranging from $2-3.5\sigma$, but it still plays a crucial role in testing the validity of ΛCDM cosmology. Recent measurements from the Kilo-Degree Survey (KiDS-1000) report a lower value of $S_8 = 0.766^{+0.020}_{-0.014}$ [49], which is consistent with other WL measurements such as DES-Y3 [50] and HSC-Y3 [51]. On the other hand, Planck (TT,TE,EE+lowE) gives $S_8 = 0.834 \pm 0.016$ [34] which agrees with other CMB based measurements of this parameter [35, 52].

The presence of cosmic tensions has spurred numerous re-evaluations in the scientific community, leading

* especogna1@sheffield.ac.uk
† e.divalentino@sheffield.ac.uk
‡ jackson.said@um.edu.mt
§ nguyenmn@umich.edu

to more rigorous investigations of potential systematic errors [25, 27, 53]. However, the persistence of these tensions across various direct and indirect measurements suggests that such explanations may be losing credibility. Consequently, alternative modifications to the standard model of cosmology have been proposed, encompassing a range of theoretical frameworks (see for example [19, 20, 24, 25, 54–61] and the references therein). This plethora of models that go beyond ΛCDM physics can be parametrized in numerous ways. By examining the phenomenological parameterization for the growth of linear matter perturbations $\delta_m = \delta\rho_m/\rho_m$ described in [62], the growth rate $G(a)$ can be approximately reformulated as $G(a) = f(a, \gamma_L, \Omega_{m,0})$, a time-dependent function f where the growth index γ_L can be seen as a fitting constant [63, 64] (discussed further in Sec. II). This empirical formula gives a value of $\gamma_L \simeq 0.55$ for ΛCDM [62, 65].

This theoretical prediction for γ_L allows us to use this parameter as a testing tool for possible deviations from the concordance model of cosmology. In this work, we analyze this parameterization through the prism of the linear matter perturbation evolution equation (Eqs. 3-4) defined in Sec. II. In Sec. III we include a discussion on the main differences in the implementation of γ_L in the two cosmological solvers considered in our study: `MGCAMB` and `CAMB_GammaPrime_Growth`. In Sec. IV we discuss the data sets under investigation, along with the strategy that we followed to obtain the constraints on the ΛCDM + γ_L model considered here, which are outlined in Sec. V, where the outcomes of both approaches are compared. In particular, the results for `MGCAMB`'s scale-dependent approach is shown in Sec. V A, along with `CAMB_GammaPrime_Growth`'s scale-independent one in Sec. V B. Finally, the main results are summarized and discussed in Sec. VI.

II. STRUCTURE FORMATION AND THE GROWTH INDEX

The dynamics of the expansion of the Universe can be determined through the Friedmann equation:

$$\left(\frac{H}{H_0}\right)^2 = \sum_i \Omega_i \,, \tag{1}$$

where $\Omega_i = \rho_i/\rho_c$ represents the relative density of each component with energy density ρ_i in a flat Universe where $\rho_c = 3H_0^2/(8\pi G_{GR})$, with G_{GR} being Newton's constant of gravitation in General Relativity (GR). Indeed we can use Eq.(1) to constrain the observed accelerated expansion, but it has to reflect our ignorance of the fundamental nature of such acceleration. Since we do not know whether we are dealing with a physical energy density or rather a modification of the Friedmann equation with respect to the ΛCDM model, we can treat the accelerated expansion as stemming from an effective component with equation of state $w(a)$, rewriting Eq.(1) as follows [63, 66]:

$$\left(\frac{H}{H_0}\right)^2 = \Omega_{\rm m,0} a^{-3} + (1-\Omega_{\rm m,0}) e^{3\int_0^{a'}[1+w(a')]d\ln a'} \,. \tag{2}$$

However, background expansion alone cannot easily tell different cosmological theories apart, as functions like $w(a)$ can be tuned in different cosmologies to obtain the same time evolution for expansion history quantities such as $a(t)$ [62]. For this reason, in this paper we will assume a ΛCDM background; namely, $w(a) = -1$ in Eq. 2.

Instead, we consider modifications to the growth of structure *only*. The evolution of the expansion rate feeds into the inhomogeneities that arise in the LSS due to early Universe gravitational instabilities and frictional terms. By investigating perturbations away from homogeneity and isotropy in both the gravitational and matter sectors, we can describe the matter perturbation evolution equation as

$$\ddot{\delta}_m + 2H\dot{\delta}_m - 4\pi\rho_m\delta_m = 0 \,, \tag{3}$$

where δ_m represents the gauge invariant fractional matter density, dots denote derivatives with respect to cosmic time, and where linear and subhorizon scales ($k \lesssim 0.1h\mathrm{Mpc}^{-1}$ and $k \gtrsim 0.0003h\mathrm{Mpc}^{-1}$ respectively, $h = H_0/100\,\mathrm{kms}^{-1}\mathrm{Mpc}^{-1}$) are being considered. A natural definition of the linear growth fraction for matter perturbations is $g(a) = \delta_m(a)/\delta_{m,0}$, where $\delta_{m,0}$ is the current value of δ_m. By taking a reparameterization of the matter perturbation evolution equation through the growth rate $G(a) = d\ln g(a)/d\ln a$, Eq. (3) can be rewritten as [67]

$$\frac{dG}{d\ln a} + G^2 + \left(2 + \frac{1}{2}\frac{d\ln H^2}{d\ln a}\right) G - \frac{3}{2} G_{\rm eff}\Omega_{\rm m}(a) = 0 \,, \tag{4}$$

where $G_{\rm eff}$ is $G_{\rm MG}/G_{\rm GR}$, and $G_{\rm MG}$ is Newton's constant of gravitation for a generic deviation from GR. It was proposed in [68] that

$$G(a) = \Omega_{\rm m}^{\gamma_L}(a) \,, \tag{5}$$

where $\gamma_L = \ln G/\ln\Omega_{\rm m}(a)$ is the *growth index*. A major advantage of this parameterization is its accuracy in replicating the numerical solution of eq.(4). For instance, in the framework of ΛCDM, the value $\gamma_L^{\Lambda\rm CDM} = 0.55$ can be as accurate as 0.05% [62].

An interesting approach considered in the literature has been to take the background Friedmann equations to be those of ΛCDM and to probe potential modifications away from the standard model at the level of γ_L [69–71]. In fact, for theories other than GR such as $f(R)$ and DGP braneworld cosmologies we get remarkably different values: $\gamma_L^{f(R)} = 0.42$ and $\gamma_L^{\rm DGP} = 0.68$ respectively [70]. A

departure of γ_L from 0.55 would then represent a possible hint at new physics, offering us an opportunity to shed new light on the tensions afflicting the standard model of cosmology.

III. MAPPING THE GROWTH INDEX INTO OBSERVABLES: MGCAMB AND CAMB_GammaPrime_Growth

To constrain the growth index γ_L, we first need a mean to map it into the CMB and LSS observables, where the latter are specifically probed by CMB lensing potentials in this work. Here, we adopt two different modifications of the standard Boltzmann solver CAMB [72, 73], namely MGCAMB [1–5] and CAMB_GammaPrime_Growth [6, 7]. Below, we briefly review the main differences between the two approaches.

In the first approach, MGCAMB introduces the two scale- and redshift-dependent parameters $\mu(a,k)$ and $\eta(a,k)$, which fully describe the relations between the Ψ- Φ metric perturbations and the energy-momentum tensor of GR, as can be observed from Eqs. (5)-(9) in [2] (with $\eta = \mu = 1$ corresponding to GR and ΛCDM). Separating sub- and super-horizon evolutions of perturbations, MGCAMB then solves the two regimes separately [2]. MGCAMB maps γ_L into the function $\mu(a,k)$ through the following relation, valid for subhorizon perturbations [2, 3]:

$$\mu = \frac{2}{3}\Omega_{\rm m}^{\gamma_L-1}\left[\Omega_{\rm m}^{\gamma_L} + 2 + \frac{H'}{H} + \gamma_L\frac{\Omega'_{\rm m}}{\Omega_{\rm m}} + \gamma'_L\ln(\Omega_{\rm m})\right]. \tag{6}$$

Therefore, within MGCAMB, any change in γ_L is effectively a change in $\mu(a,k)$, where the latter appears in the evolution of both sub- and super-horizon perturbations, as described by Eqs. (16)-(17) and Eq. (21) of [2]. This choice implies that varying γ_L introduces a *scale-dependent* effect on observables such as the primary CMB angular power spectrum and the linear matter power spectrum. Ref. [2] demonstrated that, for a simple toy model where $\mu(a,k) = \mu(a)$, super-horizon changes in the linear matter power spectrum introduced by a varying $\mu(a)$ are within the cosmic variance. They thereby argued that Eq. (6) and their approach to γ_L should be consistent with the (implicit) assumptions of scale-independence and subhorizon evolution by Eq. (5). In practice, we however find that this is not necessarily the case for the (primary) CMB angular power spectrum. In App. A, we further show why this particular choice might explain the constraint on γ_L obtained by MGCAMB in Sect. V A.[1]

The second code, CAMB_GammaPrime_Growth [6, 7, 76], adopts a phenomenological approach by rescaling the linear matter power spectrum $P(k)$, i.e.

$$P(\gamma_L, k, a) = P(k, a=1)\, D^2(\gamma_L, a), \tag{7}$$

by the (square of) the modified growth factor $D(\gamma_L, a)$ given by the numerical integral

$$D(\gamma_L, a) = \exp\left[-\int_a^1 da\,\frac{\Omega_{\rm m}^{\gamma_L}(a)}{a}\right]. \tag{8}$$

For the CMB observables and data considered in this work, Eqs. (7)–(8) only affect the CMB lensing potential through the matter transfer function (see, e.g. Eqs. (9)-(14) in [77]). We will return to this point in App. A where we compare this approach by CAMB_GammaPrime_Growth versus that by MGCAMB, and their respective constraints on γ_L using Planck(+lensing) data.

IV. DATASETS AND METHODOLOGY

Together with the growth index γ_L defined in Sec.II, we constrained the six parameters of the base ΛCDM model. The parameter space constrained here is therefore $\Gamma \equiv \{\Omega_{\rm b}h^2, \Omega_{\rm c}h^2, 100\theta_{\rm MC}, \tau_{\rm reio}, n_{\rm s}, \log(10^{10}A_{\rm s}), \gamma_L\}$, where $\Omega_b h^2$, the baryon density Ω_b combined with the dimensionless Hubble constant h, $\Omega_c h^2$, the density of cold dark matter combined with h, $100\theta_{MC}$, where θ_{MC} is an approximation of the observed angular size of the sound horizon at recombination, $\tau_{\rm reio}$, the reionization optical depth, n_s and $\log(10^{10}A_{\rm s})$, respectively the spectral index and amplitude $A_{\rm s}$ of the power spectrum of the scalar primordial perturbations.

We constrained the ΛCDM+γ_L model considered here with two different methods:

- Firstly, we used MGCosmoMC [1–5], a publicly available modification of the popular MCMC code CosmoMC [78, 79] that samples γ_L through the fast-slow dragging algorithm developed in [80]. The Einstein-Boltzmann solver implemented in MGCosmoMC to calculate CMB anisotropies and lensing power spectra is MGCAMB [1–5], a patch of the CAMB code [72] that includes several phenomenological modifications to the growth of matter perturbations, including the γ_L parameterization in Eq.(5).

- Additionally, we implemented the modified version of CAMB, namely CAMB_GammaPrime_Growth, introduced in [6, 7, 76] into CosmoMC. While [6, 7, 76] also modify linear growth through the parameterization shown in Eq.5, they take γ_L to be scale-independent compared to MGCAMB.

The data considered in our analysis have been taken from the following datasets:

- the final release of the Planck mission [34, 81, 82], specifically the likelihoods and data for the CMB temperature and polarization anisotropies: TT, EE and TE (referred to, here, as *Planck*), along with the lensing reconstruction power spectrum (referred to as *lensing*);

[1] See also Ref. [74, 75] for previous analyses with Planck data.

Parameter	Prior
$\Omega_{\rm b}h^2$	$[0.005, 0.1]$
$\Omega_{\rm c}h^2$	$[0.001, 0.99]$
$100\theta_{\rm MC}$	$[0.5, 10]$
$\tau_{\rm reio}$	0.065 ± 0.015
$n_{\rm s}$	$[0.8, 1.2]$
$\log(10^{10}A_{\rm s})$	$[1.61, 3.91]$
γ_L	$[0, 1]$

TABLE I. A summary of the priors imposed on the parameters for the ΛCDM+γ_L model considered in our analysis.

- the likelihoods and data from the 9-years release (DR9) of the Wilkinson Microwave Anisotropy Probe (*WMAP*) [83];
- the likelihoods for the polarization and temperature anisotropies spectra from Atacama Cosmology Telescope's DR4 (*ACT*) [84];
- the EE and TE anisotropies measurements and likelihoods from the SPT-3G instrument of the South Pole Telescope (*SPT*) [85];
- the final measurements from the SDSS survey by the eBOSS collaboration, of which we include Baryonic Acoustic Oscillations (*BAO*) data [86].

In particular, we constrained Γ with the following combinations:

- Planck, Planck+BAO, Planck+lensing, and Planck+BAO+lensing;
- ACT, ACT+WMAP, ACT+BAO and ACT+WMAP+BAO;
- SPT, SPT+WMAP, SPT+BAO and SPT+WMAP+BAO.

We note that all the constraints obtained using either the ACT or SPT data employed a Gaussian prior on $\tau_{reio} = 0.065 \pm 0.015$, as done by the ACT collaboration [84]; the other six parameters making up the ΛCDM+γ_L model considered here were all assumed to have flat priors, as summarised in Table I .

The convergence of the chains produced from the exploration of Γ by `MGCosmoMC/CosmoMC` for this analysis was evaluated through the Gelman-Rubin criterion [87], and we took $R \leq 0.02$ as a satisfactory limit at which to present the results outlined in Sec.V.

Finally, to demonstrate that a Planck-like CMB only experiment is able to recover $\gamma_L = 0.55$ without bias, we constrained Γ using a mock Planck-like dataset generated according to a ΛCDM model defined by the parameter choices given in Table II. The results are shown in Table III, and we can see that CMB only data are able to recover $\gamma_L = 0.55$ with good accuracy with either `MGCAMB` or `CAMB_GammaPrime_Growth`.

Parameter	Fiducial Values
$\Omega_{\rm b}h^2$	0.02236
$\Omega_{\rm c}h^2$	0.1202
$100\theta_{\rm MC}$	1.04090
$\tau_{\rm reio}$	0.0544
$n_{\rm s}$	0.9649
$\log(10^{10}A_{\rm s})$	3.044

TABLE II. The ΛCDM baseline values chosen to simulate mock Planck-like dataset used for the results of Table III.

Parameter	`MGCAMB`	`CAMB_GammaPrime_Growth`
$\Omega_b h^2$	0.02237 ± 0.00015	0.02236 ± 0.00016
$\Omega_c h^2$	0.1201 ± 0.0016	0.1202 ± 0.0017
$100\theta_{MC}$	1.04091 ± 0.00036	1.04089 ± 0.00036
τ	0.0538 ± 0.0097	0.053 ± 0.010
n_s	0.9650 ± 0.0041	0.9649 ± 0.0043
$\log(10^{10}A_{\rm s})$	3.044 ± 0.019	3.043 ± 0.021
γ_L	$0.544^{+0.035}_{-0.021}$	0.56 ± 0.10

TABLE III. Results for the Planck-like dataset.

V. RESULTS

In this section we are discussing the constraints we obtained for the dataset combinations listed in the previous section IV and the two different approaches explained in section III. In particular we will discuss in section V A the scale-dependent case as implemented in `MGCAMB`, and in section V B the scale-independent linear growth as implemented in `CAMB_GammaPrime_Growth`.

A. MGCAMB Results

We show in Table IV the constraints at 68% CL for the scale-dependent case as implemented in `MGCAMB` for the different combinations involving the Planck data, and we repeat the same for ACT in Table V and SPT in Table VI. We display instead the 1D posterior distributions and the 2D contour plots for all these cases in Figure 1 and Figure 2.

The analysis presented in Table IV reveals a notable deviation from the expected value of $\gamma_L = 0.55$ considering the measurement obtained solely from Planck observations. Specifically, Planck indicates a value of $\gamma_L = 0.467^{+0.018}_{-0.029}$, deviating from the expected value by more than 3 standard deviations. However, it is important to note that this parameter does not contribute significantly to resolving the cosmological tensions. While it exhibits a slight correlation with H_0, resulting in a modest increase of only 1σ in its value ($H_0 = 68.02 \pm 0.66$ km/s/Mpc), it does not exhibit any correlation with S_8 (see Figure 1). Notably, the disagreement between WL measurements (which assume a ΛCDM model) and S_8 persists, further emphasizing the unresolved tensions in

Parameter	Planck	Planck+BAO	Planck+lensing	Planck+BAO+lensing
$\Omega_{\rm b}h^2$	0.02253 ± 0.00016	0.02250 ± 0.00016	0.02249 ± 0.00016	0.02246 ± 0.00015
$\Omega_{\rm c}h^2$	0.1187 ± 0.0015	0.1190 ± 0.0013	0.1186 ± 0.0014	0.1189 ± 0.0012
$100\theta_{\rm MC}$	1.04110 ± 0.00032	1.04106 ± 0.00032	1.04107 ± 0.00032	1.04103 ± 0.00030
τ_{reio}	0.0510 ± 0.0085	0.0507 ± 0.0082	$0.0496^{+0.0087}_{-0.0073}$	$0.0490^{+0.0083}_{-0.0073}$
$n_{\rm s}$	0.9688 ± 0.0047	0.9681 ± 0.0045	0.9684 ± 0.0046	0.9675 ± 0.0042
$\log(10^{10}A_{\rm s})$	3.034 ± 0.018	3.034 ± 0.017	$3.030^{+0.018}_{-0.015}$	3.030 ± 0.017
γ_L	$0.467^{+0.018}_{-0.029}$	$0.469^{+0.017}_{-0.029}$	0.506 ± 0.022	$0.509^{+0.022}_{-0.020}$
H_0	68.02 ± 0.66	67.86 ± 0.60	68.00 ± 0.64	67.84 ± 0.57
S_8	0.839 ± 0.015	0.842 ± 0.015	0.824 ± 0.013	0.827 ± 0.012

TABLE IV. Constraints at 68% CL for the scale-dependent case as implemented in `MGCAMB`, considering the dataset combinations with Planck.

Parameter	ACT	ACT+BAO	ACT+WMAP	ACT+WMAP+BAO
$\Omega_{\rm b}h^2$	0.02153 ± 0.00032	0.02148 ± 0.00030	0.02239 ± 0.00021	0.02237 ± 0.00019
$\Omega_{\rm c}h^2$	0.1177 ± 0.0049	0.1200 ± 0.0025	0.1198 ± 0.0027	0.1203 ± 0.0020
$100\theta_{\rm MC}$	1.04229 ± 0.00078	1.04210 ± 0.00065	1.04174 ± 0.00066	1.04171 ± 0.00062
τ_{reio}	0.064 ± 0.015	0.065 ± 0.015	0.060 ± 0.012	0.060 ± 0.012
$n_{\rm s}$	1.008 ± 0.017	1.003 ± 0.014	0.9729 ± 0.0062	0.9722 ± 0.0052
$\log(10^{10}A_{\rm s})$	3.049 ± 0.034	3.056 ± 0.033	$3.062^{+0.025}_{-0.022}$	$3.064^{+0.025}_{-0.022}$
γ_L	$0.552^{+0.063}_{-0.087}$	$0.580^{+0.062}_{-0.078}$	$0.533^{+0.044}_{-0.018}$	$0.536^{+0.040}_{-0.018}$
H_0	68.0 ± 2.0	67.0 ± 1.0	67.7 ± 1.1	67.50 ± 0.83
S_8	0.829 ± 0.045	0.847 ± 0.028	0.843 ± 0.031	0.848 ± 0.025

TABLE V. Constraints at 68% CL for the scale-dependent case as implemented in `MGCAMB`, considering the dataset combinations with ACT.

the current cosmological framework. Even when incorporating BAO data, the same conclusion holds true. The inclusion of BAO data does not alter the constraints on γ_L and S_8, but it does lead to a slight decrease in the estimated value of H_0. However, a more significant impact is observed when including the lensing dataset. Specifically, with Planck+lensing the constraint on γ_L becomes $\gamma_L = 0.506 \pm 0.022$, reducing the tension with the expected value to 2σ. Furthermore, a mild correlation emerges between the γ_L parameter and the S_8 parameter (see Figure 1). This correlation causes the mean value of S_8 to shift downward by 1 standard deviation, albeit not sufficiently enough to alleviate the existing S_8 tension. Once again, the inclusion of BAO data does not change the results, so that Planck+BAO+lensing gives similar constraints to the Planck+lensing combination.

A different picture emerges when the ground based CMB telescope ACT is taken into account in Table V. In this case, the value of γ_L remains consistently within 1 standard deviation of the expected value across all dataset combinations, including also BAO and WMAP data. Furthermore, by referring to Figure 1 and Figure 2, we observe a change: the correlation between γ_L and other cosmological parameters disappears upon inclusion of the ACT data.

Similarly, when the SPT data are analyzed in Table VI we observe that across all combinations of datasets γ_L is always in agreement within 1σ with $\gamma_L = 0.55$. In particular, when considering SPT data alone, or in combination with BAO data, higher values of γ_L are favored with larger error bars. However, upon including the WMAP dataset, the mean value of γ_L returns to $\gamma_L = 0.55$. Similar to the previous analysis, no correlation is observed between γ_L and the derived parameters depicted in Figure 1 and Figure 2 when examining this dataset.

B. `CAMB_GammaPrime_Growth` Results

The constraints at a confidence level of 68% CL for the `CAMB_GammaPrime_Growth` case as implemented in [6, 7, 76], are presented in Table VII, for the various combinations involving Planck data. Similarly, we provide the corresponding constraints for ACT in Table VIII and for SPT in Table IX. To further illustrate these cases, we present the 1D posterior distributions and

Parameter	SPT	SPT+BAO	SPT+WMAP	SPT+WMAP+BAO
$\Omega_{\rm b}h^2$	0.02238 ± 0.00033	0.02237 ± 0.00032	0.02264 ± 0.00023	0.02259 ± 0.00021
$\Omega_c h^2$	0.1175 ± 0.0057	0.1186 ± 0.0026	0.1153 ± 0.0028	0.1171 ± 0.0020
$100\theta_{\rm MC}$	1.03945 ± 0.00081	1.03933 ± 0.00069	1.03973 ± 0.00066	1.03954 ± 0.00064
τ_{reio}	0.065 ± 0.015	0.066 ± 0.015	0.060 ± 0.013	0.058 ± 0.013
$n_{\rm s}$	0.991 ± 0.025	0.987 ± 0.019	0.9733 ± 0.0075	0.9709 ± 0.0067
$\log(10^{10}A_{\rm s})$	3.040 ± 0.039	3.043 ± 0.038	3.041 ± 0.025	3.042 ± 0.026
γ_L	$0.622^{+0.075}_{-0.11}$	$0.635^{+0.063}_{-0.084}$	$0.556^{+0.023}_{-0.018}$	$0.558^{+0.024}_{-0.018}$
H_0	67.8 ± 2.3	67.3 ± 1.0	68.9 ± 1.2	68.11 ± 0.83
S_8	0.796 ± 0.048	0.804 ± 0.028	0.782 ± 0.032	0.801 ± 0.025

TABLE VI. Constraints at 68% CL for the scale-dependent case as implemented in `MGCAMB`, considering the dataset combinations with SPT.

Parameter	Planck	Planck+BAO	Planck+lensing	Planck+BAO+lensing
$\Omega_{\rm b}h^2$	0.02258 ± 0.00016	0.02255 ± 0.00016	0.02251 ± 0.00017	0.02248 ± 0.00016
$\Omega_c h^2$	0.1181 ± 0.0015	0.1186 ± 0.0013	0.1183 ± 0.0015	0.1188 ± 0.0013
$100\theta_{\rm MC}$	1.04113 ± 0.00032	1.04108 ± 0.00031	1.04109 ± 0.00032	1.04103 ± 0.00032
$\tau_{\rm reio}$	$0.0496^{+0.0087}_{-0.0074}$	0.0495 ± 0.0084	$0.0493^{+0.0087}_{-0.0074}$	$0.0488^{+0.0086}_{-0.0075}$
$n_{\rm s}$	0.9709 ± 0.0047	0.9696 ± 0.0045	0.9696 ± 0.0048	0.9683 ± 0.0044
$\log(10^{10}A_{\rm s})$	3.030 ± 0.017	3.031 ± 0.018	$3.029^{+0.018}_{-0.016}$	$3.029^{+0.018}_{-0.016}$
γ_L	$0.841^{+0.11}_{-0.074}$	$0.831^{+0.11}_{-0.080}$	0.669 ± 0.069	0.658 ± 0.063
H_0	68.27 ± 0.69	68.06 ± 0.61	68.14 ± 0.70	67.92 ± 0.61
S_8	0.805 ± 0.018	0.810 ± 0.017	0.807 ± 0.019	0.812 ± 0.017

TABLE VII. Constraints at 68% CL for the `CAMB_GammaPrime_Growth` case as implemented in [6, 7, 76], considering the dataset combinations with Planck.

the 2D contour plots in Figure 3 and Figure 4.

The examination of Table VII reveals a significant deviation from the expected value of $\gamma_L = 0.55$ when considering the measurement based solely on Planck observations. Specifically, Planck indicates a value of $\gamma_L = 0.841^{+0.11}_{-0.074}$, surpassing the expected value by more than 3σ. However, it is worth noting that while this parameter does not contribute significantly to resolving the H_0 tension, it can substantially decrease the value of the S_8 parameter in the right direction to agree with the WL measurements (which assume a ΛCDM model). In fact, contrarily to the `MGCAMB` case, γ_L exhibits a slight correlation with both H_0 and S_8 (see Figure 3), giving $H_0 = 68.27 \pm 0.69$ km/s/Mpc and $S_8 = 0.805 \pm 0.018$. It is important to emphasize that in the `CAMB_GammaPrime_Growth` case, there are two notable distinctions. Firstly, the preferred value of γ_L deviates from the expected value in the opposite direction compared to the `MGCAMB` case. Secondly, the correlations between γ_L, H_0, and S_8 exhibit a change in sign. However, as we noted in the previous section as well, the inclusion of the CMB lensing dataset is crucial to shift the value of γ_L towards the expected $\gamma_L = 0.55$, reducing the disagreement at the level of 1.7σ. In particular we obtain $\gamma_L = 0.669 \pm 0.069$, in perfect agreement with [6], while leaving both H_0 and S_8 unaffected. Finally, the addition of the BAO data does not have a significant impact on either the Planck+BAO combination or the Planck+BAO+lensing combination.

If we now consider the independent CMB measurements obtained from ACT displayed in Table VIII we observe a similar pattern as in the previous section. Notably, γ_L returns to agree within 1σ with the expected value $\gamma_L = 0.55$. In this case the addition of BAO and WMAP data does not alter these conclusions. In this particular dataset combination, γ_L exhibits a negative correlation with S_8 and a positive degeneracy with H_0. However, their mean values remain robust and align with the values expected in a ΛCDM model, in absence of deviations in γ_L from 0.55. The same conclusions about constraints and parameter degeneracies remain valid when replacing ACT with SPT, as demonstrated in Table IX.

In conclusion, the observed deviation of γ_L when analyzing the Planck data can be attributed to the presence of the $A_{\rm lens}$ problem [34, 88, 89], as highlighted in [6]. This problem refers to the excess of lensing detected in

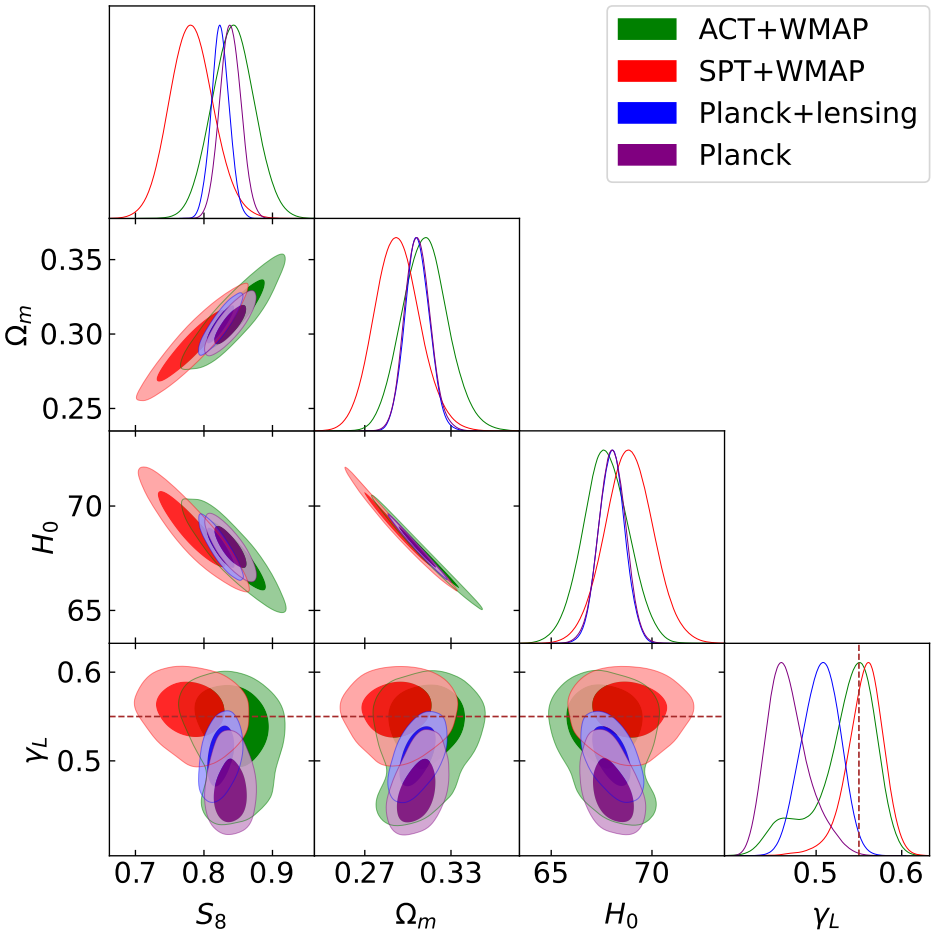


FIG. 1. 1D marginalized posterior distributions and 2D contour plots for the different CMB data combinations explored in this work, without the inclusion of the BAO data, for the scale-dependent case as implemented in `MGCAMB`. The dashed brown line in the plot is the value of the growth index in ΛCDM, $\gamma_L = 0.55$.

the temperature power spectrum, which is also associated with indications of a closed Universe [34, 90, 91]. The mitigation of the γ_L deviation from 0.55 upon incorporating the CMB lensing data serves as direct evidence supporting this interpretation.

VI. CONCLUSIONS

We investigated the growth index γ_L, which characterizes the growth of linear matter perturbations in the form shown in Eq. (5), by using different cosmological datasets, and comparing two approaches for the implementation of γ_L into `CAMB`: the `MGCAMB` and `CAMB_GammaPrime_Growth` codes.

Our analysis in the `MGCAMB` case revealed a γ_L that deviates from its ΛCDM value of 0.55, preferring instead lower values and indicating a discrepancy of more than 3 standard deviations. However, incorporating the CMB lensing dataset helps reduce this disagreement to approximately 2 standard deviations.

In the `CAMB_GammaPrime_Growth` case instead, the preferred value of γ_L differs from the `MGCAMB` case, and exceeds the expected value in the opposite direction, producing a change of sign of the correlations with H_0 and S_8. Similarly to `MGCAMB`, for the `CAMB_GammaPrime_Growth` case the CMB lensing dataset helps in reconciling γ_L with the expected 0.55 value.

Moreover, the analysis of the ACT and SPT datasets shows consistent agreement of γ_L with the expected value within 1 standard deviation across various dataset combinations, and the addition of BAO data has minimal impact on the constraints and parameter correlations in both the `MGCAMB` and `CAMB_GammaPrime_Growth` cases.

Given these facts, we can attribute the deviation of γ_L observed in the Planck dataset to the $A_{\rm lens}$ problem (as already noticed in [6]) characterized by excess lensing in the temperature power spectrum.

Overall, these findings highlight the importance of considering additional datasets, such as CMB lensing, and other experiments, such as ACT and SPT, when tackling

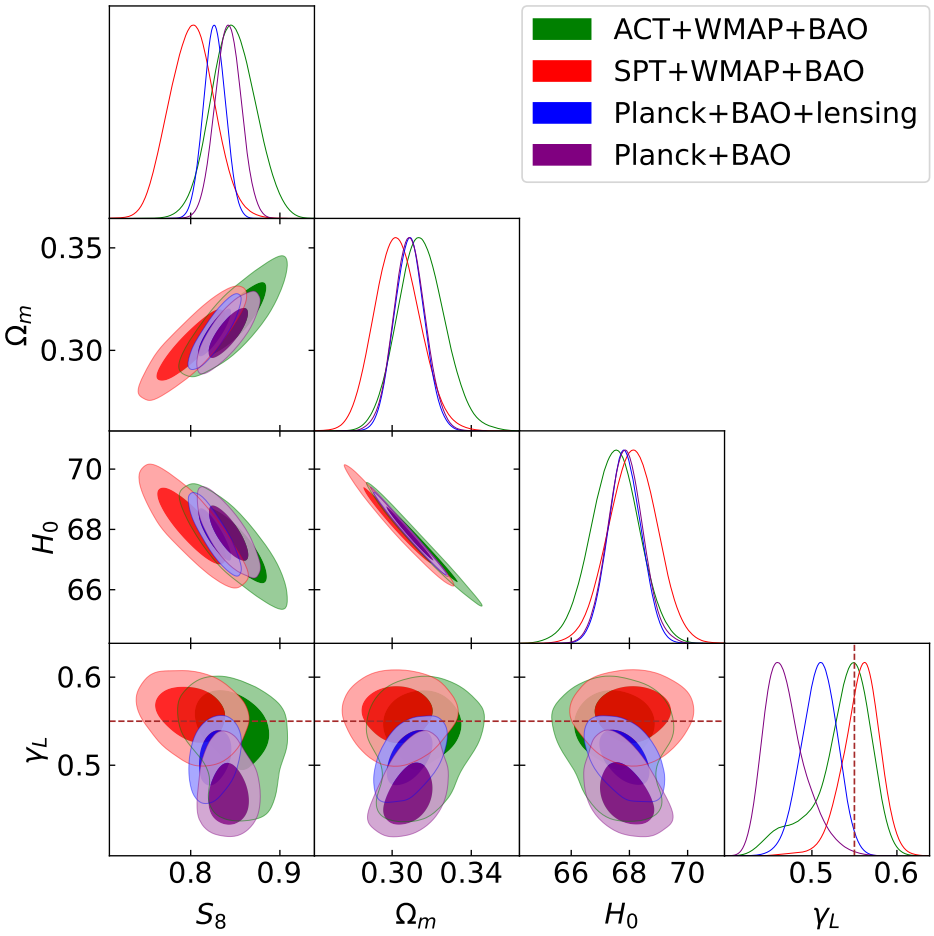


FIG. 2. 1D marginalized posterior distributions and 2D contour plots for the different CMB+BAO data combinations explored in this work, for the scale-dependent case as implemented in `MGCAMB`. The dashed brown line in the plot is the value of the growth index in ΛCDM, $\gamma_L = 0.55$.

apparent discrepancies with the standard model, such as the deviations of γ_L encountered in this work.

ACKNOWLEDGMENTS

This article is based upon work from COST Action CA21136 Addressing observational tensions in cosmology with systematics and fundamental physics (CosmoVerse) supported by COST (European Cooperation in Science and Technology). We would like to thank the referee for their constructive feedback and helpful comments. We acknowledge IT Services at The University of Sheffield for the provision of services for High Performance Computing. The `MGCAMB-CAMB_GammaPrime_Growth` code verification and comparison was performed on the Great Lakes HPC cluster, maintained by the Advanced Research Computing division, UofM Information and Technology Service. We further thank Dragan Huterer, Levon Pogosian, Alessandra Silvestri and Zhuangfei (Xavier) Wang for helpful discussions related to `MGCAMB` and their implementation of γ_L. EDV is supported by a Royal Society Dorothy Hodgkin Research Fellowship. MN acknowledges support from the Leinweber Center for Theoretical Physics, the NASA grant under contract 19-ATP19-0058, and the DOE under contract DE-FG02-95ER40899. JLS would also like to acknowledge funding from "The Malta Council for Science and Technology" as part of the REP-2023-019 (CosmoLearn) Project.

[1] G.-B. Zhao, L. Pogosian, A. Silvestri, and J. Zylberberg, Phys. Rev. D **79**, 083513 (2009), arXiv:0809.3791 [astro-ph].

[2] L. Pogosian, A. Silvestri, K. Koyama, and G.-B. Zhao, Phys. Rev. D **81**, 104023 (2010), arXiv:1002.2382 [astro-ph.CO].

Parameter	ACT	ACT+BAO	ACT+WMAP	ACT+WMAP+BAO
$\Omega_{\rm b}h^2$	0.02151 ± 0.00031	0.02149 ± 0.00031	0.02236 ± 0.00021	0.02235 ± 0.00020
$\Omega_c h^2$	0.1185 ± 0.0050	0.1199 ± 0.0026	0.1205 ± 0.0030	0.1206 ± 0.0022
$100\theta_{\rm MC}$	1.04221 ± 0.00077	1.04205 ± 0.00065	1.04168 ± 0.00066	1.04164 ± 0.00060
τ_{reio}	0.065 ± 0.015	0.065 ± 0.015	0.062 ± 0.013	0.061 ± 0.013
$n_{\rm s}$	1.007 ± 0.017	1.003 ± 0.014	0.9722 ± 0.0066	0.9720 ± 0.0055
$\log(10^{10}A_{\rm s})$	3.053 ± 0.034	3.057 ± 0.032	3.067 ± 0.026	3.067 ± 0.026
γ_L	0.52 ± 0.18	0.49 ± 0.15	0.50 ± 0.16	0.50 ± 0.14
H_0	67.7 ± 2.0	67.1 ± 1.0	67.4 ± 1.3	67.39 ± 0.89
S_8	0.839 ± 0.059	0.855 ± 0.032	0.847 ± 0.036	0.848 ± 0.027

TABLE VIII. Constraints at 68% CL for the `CAMB_GammaPrime_Growth` case as implemented in [6, 7, 76], considering the dataset combinations with ACT.

Parameter	SPT	SPT+BAO	SPT+WMAP	SPT+WMAP+BAO
$\Omega_{\rm b}h^2$	0.02241 ± 0.00033	0.02238 ± 0.00031	0.02259 ± 0.00024	0.02253 ± 0.00022
$\Omega_c h^2$	0.1164 ± 0.0056	0.1183 ± 0.0026	0.1167 ± 0.0032	0.1178 ± 0.0021
$100\theta_{\rm MC}$	1.03953 ± 0.00081	1.03935 ± 0.00067	1.03955 ± 0.00071	1.03942 ± 0.00064
τ_{reio}	0.065 ± 0.015	0.065 ± 0.015	0.062 ± 0.013	0.061 ± 0.013
$n_{\rm s}$	0.994 ± 0.024	0.989 ± 0.019	0.9709 ± 0.0080	0.9687 ± 0.0068
$\log(10^{10}A_{\rm s})$	3.035 ± 0.039	3.040 ± 0.035	3.049 ± 0.027	3.051 ± 0.027
γ_L	0.46 ± 0.19	0.41 ± 0.15	0.43 ± 0.14	0.41 ± 0.13
H_0	$68.3^{+2.1}_{-2.4}$	67.4 ± 1.0	68.3 ± 1.4	67.77 ± 0.89
S_8	0.803 ± 0.064	0.824 ± 0.032	0.802 ± 0.039	0.815 ± 0.027

TABLE IX. Constraints at 68% CL for the `CAMB_GammaPrime_Growth` case as implemented in [6, 7, 76], considering the dataset combinations with SPT.

[3] A. Hojjati, L. Pogosian, and G.-B. Zhao, JCAP **08**, 005, arXiv:1106.4543 [astro-ph.CO].
[4] A. Zucca, L. Pogosian, A. Silvestri, and G.-B. Zhao, JCAP **05**, 001, arXiv:1901.05956 [astro-ph.CO].
[5] Z. Wang, S. H. Mirpoorian, L. Pogosian, A. Silvestri, and G.-B. Zhao, (2023), arXiv:2305.05667 [astro-ph.CO].
[6] N.-M. Nguyen, D. Huterer, and Y. Wen, (2023), arXiv:2302.01331 [astro-ph.CO].
[7] Y. Wen, N.-M. Nguyen, and D. Huterer, (2023), arXiv:2304.07281 [astro-ph.CO].
[8] P. J. E. Peebles and B. Ratra, Rev. Mod. Phys. **75**, 559 (2003), arXiv:astro-ph/0207347.
[9] V. Mukhanov, *Physical Foundations of Cosmology* (Cambridge Univ. Press, Cambridge, 2005).
[10] B. Carr, F. Kuhnel, and M. Sandstad, Phys. Rev. D **94**, 083504 (2016), arXiv:1607.06077 [astro-ph.CO].
[11] D. S. Akerib *et al.* (LUX), Phys. Rev. Lett. **118**, 021303 (2017), arXiv:1608.07648 [astro-ph.CO].
[12] R. J. Gaitskell, Ann. Rev. Nucl. Part. Sci. **54**, 315 (2004).
[13] A. G. Riess *et al.* (Supernova Search Team), Astron. J. **116**, 1009 (1998), arXiv:astro-ph/9805201.
[14] S. Perlmutter *et al.* (Supernova Cosmology Project), Astrophys. J. **517**, 565 (1999), arXiv:astro-ph/9812133.
[15] A. H. Guth, Phys. Rev. D **23**, 347 (1981).
[16] A. D. Linde, Phys. Lett. B **108**, 389 (1982).
[17] S. Weinberg, Rev. Mod. Phys. **61**, 1 (1989).
[18] E. J. Copeland, M. Sami, and S. Tsujikawa, Int. J. Mod. Phys. D **15**, 1753 (2006), arXiv:hep-th/0603057.
[19] A. Addazi *et al.*, Prog. Part. Nucl. Phys. **125**, 103948 (2022), arXiv:2111.05659 [hep-ph].
[20] E. Abdalla *et al.*, JHEAp **34**, 49 (2022), arXiv:2203.06142 [astro-ph.CO].
[21] E. Di Valentino *et al.*, Astropart. Phys. **131**, 102606 (2021), arXiv:2008.11283 [astro-ph.CO].
[22] E. Di Valentino *et al.*, Astropart. Phys. **131**, 102604 (2021), arXiv:2008.11285 [astro-ph.CO].
[23] D. Staicova, in *16th Marcel Grossmann Meeting on Recent Developments in Theoretical and Experimental General Relativity, Astrophysics and Relativistic Field Theories* (2021) arXiv:2111.07907 [astro-ph.CO].
[24] E. Di Valentino, O. Mena, S. Pan, L. Visinelli, W. Yang, A. Melchiorri, D. F. Mota, A. G. Riess, and J. Silk, Class. Quant. Grav. **38**, 153001 (2021), arXiv:2103.01183 [astro-ph.CO].
[25] L. Perivolaropoulos and F. Skara, New Astron. Rev. **95**, 101659 (2022), arXiv:2105.05208 [astro-ph.CO].
[26] E. Di Valentino, W. Giarè, A. Melchiorri, and J. Silk, Phys. Rev. D **106**, 103506 (2022), arXiv:2209.12872 [astro-ph.CO].
[27] E. Di Valentino *et al.*, Astropart. Phys. **131**, 102605

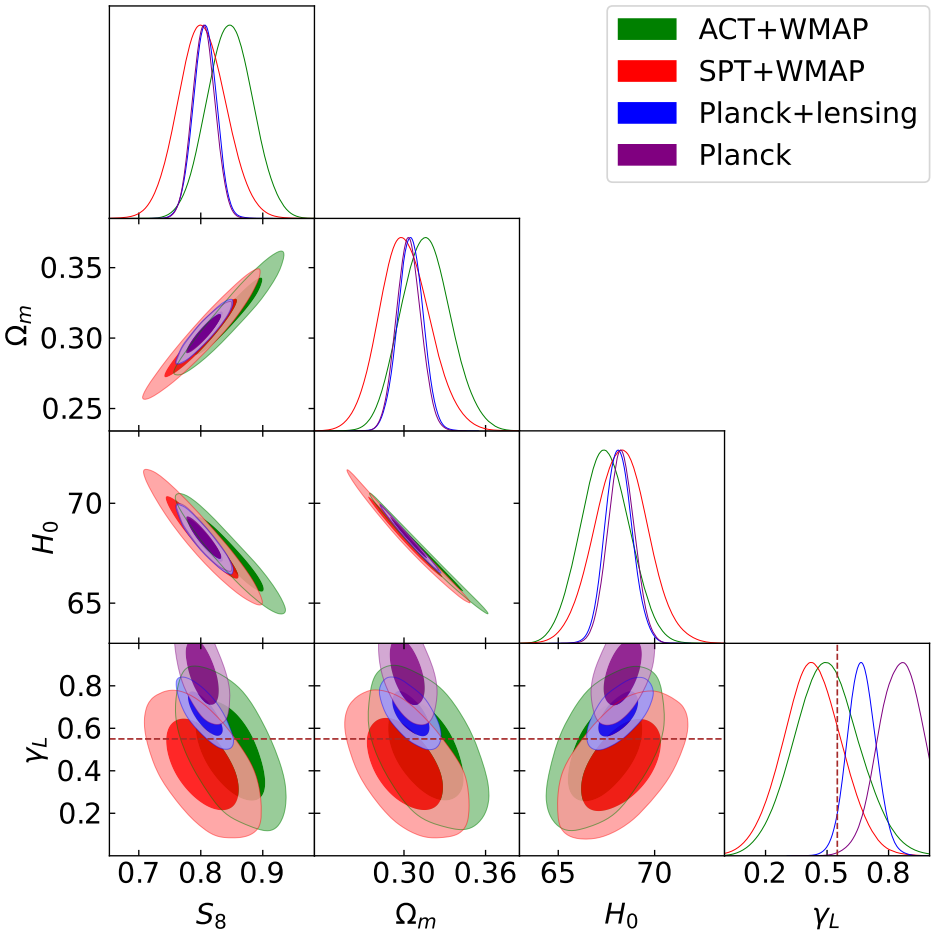


FIG. 3. 1D marginalized posterior distributions and 2D contour plots for the different CMB data combinations explored in this work, without the inclusion of the BAO data, for the `CAMB_GammaPrime_Growth` case as implemented in [6, 7, 76]. The dashed brown line in the plot is the value of the growth index in ΛCDM, $\gamma_L = 0.55$.

(2021), arXiv:2008.11284 [astro-ph.CO].
[28] M. Sajjad Athar *et al.*, Prog. Part. Nucl. Phys. **124**, 103947 (2022), arXiv:2111.07586 [hep-ph].
[29] R. C. Nunes and S. Vagnozzi, Mon. Not. Roy. Astron. Soc. **505**, 5427 (2021), arXiv:2106.01208 [astro-ph.CO].
[30] L. Verde, T. Treu, and A. G. Riess, Nature Astron. **3**, 891 (2019), arXiv:1907.10625 [astro-ph.CO].
[31] E. Di Valentino, Mon. Not. Roy. Astron. Soc. **502**, 2065 (2021), arXiv:2011.00246 [astro-ph.CO].
[32] A. G. Riess, Nature Rev. Phys. **2**, 10 (2019), arXiv:2001.03624 [astro-ph.CO].
[33] A. G. Riess, L. Breuval, W. Yuan, S. Casertano, L. M. Macri, J. B. Bowers, D. Scolnic, T. Cantat-Gaudin, R. I. Anderson, and M. C. Reyes, Astrophys. J. **938**, 36 (2022), arXiv:2208.01045 [astro-ph.CO].
[34] N. Aghanim *et al.* (Planck), Astron. Astrophys. **641**, A6 (2020), [Erratum: Astron.Astrophys. 652, C4 (2021)], arXiv:1807.06209 [astro-ph.CO].
[35] S. Aiola *et al.* (ACT), JCAP **12**, 047, arXiv:2007.07288 [astro-ph.CO].
[36] A. G. Riess *et al.*, Astrophys. J. Lett. **934**, L7 (2022), arXiv:2112.04510 [astro-ph.CO].
[37] K. C. Wong *et al.*, Mon. Not. Roy. Astron. Soc. **498**, 1420 (2020), arXiv:1907.04869 [astro-ph.CO].
[38] C. D. Huang, A. G. Riess, W. Yuan, L. M. Macri, N. L. Zakamska, S. Casertano, P. A. Whitelock, S. L. Hoffmann, A. V. Filippenko, and D. Scolnic 10.3847/1538-4357/ab5dbd (2019), arXiv:1908.10883 [astro-ph.CO].
[39] D. W. Pesce *et al.*, Astrophys. J. Lett. **891**, L1 (2020), arXiv:2001.09213 [astro-ph.CO].
[40] E. Kourkchi, R. B. Tully, G. S. Anand, H. M. Courtois, A. Dupuy, J. D. Neill, L. Rizzi, and M. Seibert, Astrophys. J. **896**, 3 (2020), arXiv:2004.14499 [astro-ph.GA].
[41] J. Schombert, S. McGaugh, and F. Lelli, Astron. J. **160**, 71 (2020), arXiv:2006.08615 [astro-ph.CO].
[42] J. P. Blakeslee, J. B. Jensen, C.-P. Ma, P. A. Milne, and J. E. Greene, Astrophys. J. **911**, 65 (2021), arXiv:2101.02221 [astro-ph.CO].
[43] T. de Jaeger, L. Galbany, A. G. Riess, B. E. Stahl, B. J. Shappee, A. V. Filippenko, and W. Zheng, Mon. Not. Roy. Astron. Soc. **514**, 4620 (2022), arXiv:2203.08974 [astro-ph.CO].
[44] A. J. Shajib *et al.*, Astron. Astrophys. **673**, A9 (2023), arXiv:2301.02656 [astro-ph.CO].
[45] D. Scolnic, A. G. Riess, J. Wu, S. Li, G. S. Anand, R. Beaton, S. Casertano, R. Anderson, S. Dhawan, and

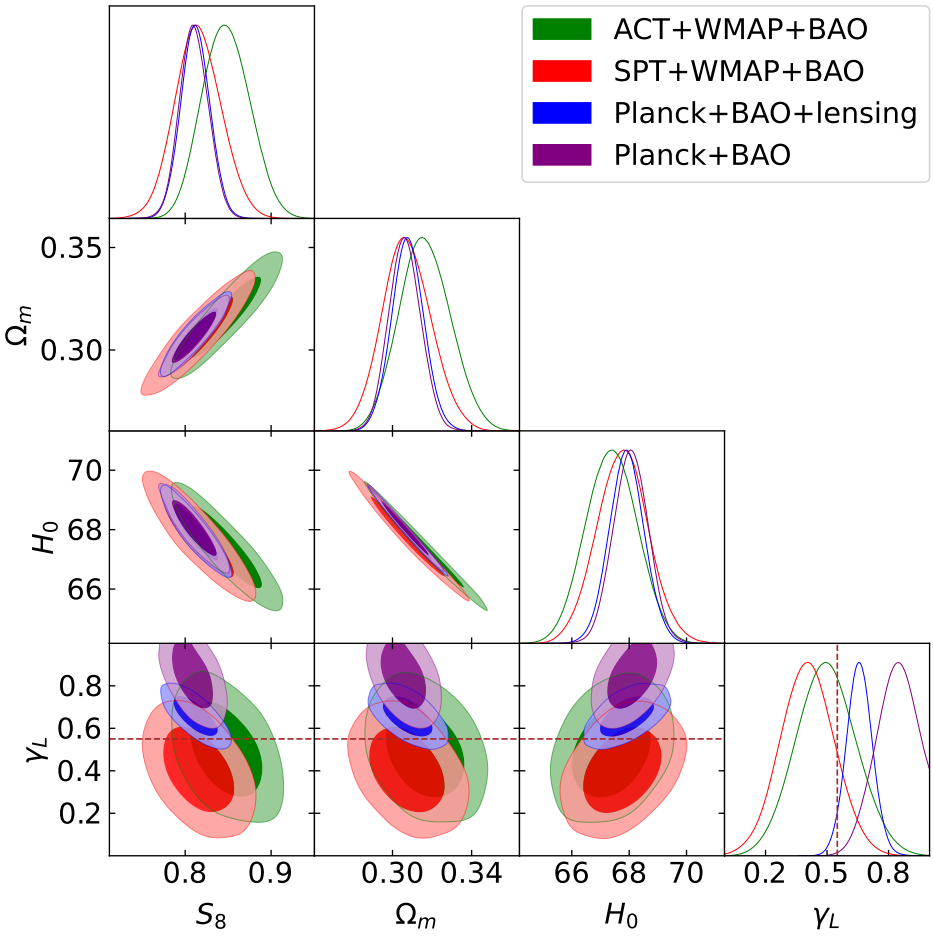


FIG. 4. 1D marginalized posterior distributions and 2D contour plots for the different CMB+BAO data combinations explored in this work, for the `CAMB_GammaPrime_Growth` case as implemented in [6, 7, 76]. The dashed brown line in the plot is the value of the growth index in ΛCDM, $\gamma_L = 0.55$.

X. Ke, (2023), arXiv:2304.06693 [astro-ph.CO].
[46] R. I. Anderson, N. W. Koblischke, and L. Eyer, (2023), arXiv:2303.04790 [astro-ph.CO].
[47] W. L. Freedman, Astrophys. J. **919**, 16 (2021), arXiv:2106.15656 [astro-ph.CO].
[48] W. L. Freedman, B. F. Madore, T. Hoyt, I. S. Jang, R. Beaton, M. G. Lee, A. Monson, J. Neeley, and J. Rich 10.3847/1538-4357/ab7339 (2020), arXiv:2002.01550 [astro-ph.GA].
[49] C. Heymans *et al.*, Astron. Astrophys. **646**, A140 (2021), arXiv:2007.15632 [astro-ph.CO].
[50] T. M. C. Abbott *et al.* (DES), Phys. Rev. D **105**, 023520 (2022), arXiv:2105.13549 [astro-ph.CO].
[51] R. Dalal *et al.*, (2023), arXiv:2304.00701 [astro-ph.CO].
[52] L. Balkenhol *et al.* (SPT-3G), (2022), arXiv:2212.05642 [astro-ph.CO].
[53] D. Brout *et al.*, Astrophys. J. **938**, 111 (2022), arXiv:2112.03864 [astro-ph.CO].
[54] L. Knox and M. Millea, Phys. Rev. D **101**, 043533 (2020), arXiv:1908.03663 [astro-ph.CO].
[55] K. Jedamzik, L. Pogosian, and G.-B. Zhao, Commun. in Phys. **4**, 123 (2021), arXiv:2010.04158 [astro-ph.CO].
[56] V. Poulin, T. L. Smith, and T. Karwal, (2023), arXiv:2302.09032 [astro-ph.CO].
[57] E. Di Valentino, Universe **8**, 399 (2022).
[58] C. Krishnan, E. O. Colgáin, M. M. Sheikh-Jabbari, and T. Yang, Phys. Rev. D **103**, 103509 (2021), arXiv:2011.02858 [astro-ph.CO].
[59] S. A. Adil, O. Akarsu, M. Malekjani, E. O. Colgáin, S. Pourojaghi, A. A. Sen, and M. M. Sheikh-Jabbari, (2023), arXiv:2303.06928 [astro-ph.CO].
[60] E. N. Saridakis *et al.* (CANTATA), (2021), arXiv:2105.12582 [gr-qc].
[61] M. Kamionkowski and A. G. Riess, (2022), arXiv:2211.04492 [astro-ph.CO].
[62] E. V. Linder, Phys. Rev. D **72**, 043529 (2005), arXiv:astro-ph/0507263.
[63] E. V. Linder and A. Jenkins, Mon. Not. Roy. Astron. Soc. **346**, 573 (2003), arXiv:astro-ph/0305286.
[64] E. V. Linder, Phys. Rev. Lett. **90**, 091301 (2003), arXiv:astro-ph/0208512.
[65] L.-M. Wang and P. J. Steinhardt, Astrophys. J. **508**, 483 (1998), arXiv:astro-ph/9804015.
[66] E. V. Linder, Phys. Rev. D **70**, 023511 (2004), arXiv:astro-ph/0402503.
[67] E. V. Linder and D. Polarski, Phys. Rev. D **99**, 023503

(2019), arXiv:1810.10547 [astro-ph.CO].
[68] E. V. Linder and R. N. Cahn, Astropart. Phys. **28**, 481 (2007), arXiv:astro-ph/0701317.
[69] E. V. Linder, AIP Conf. Proc. **655**, 193 (2003), arXiv:astro-ph/0302038.
[70] E. V. Linder, (2023), arXiv:2304.04803 [astro-ph.CO].
[71] E. V. Linder, Astropart. Phys. **26**, 102 (2006), arXiv:astro-ph/0604280.
[72] A. Lewis, A. Challinor, and A. Lasenby, Astrophys. J. **538**, 473 (2000), arXiv:astro-ph/9911177.
[73] C. Howlett, A. Lewis, A. Hall, and A. Challinor, JCAP **04**, 027, arXiv:1201.3654 [astro-ph.CO].
[74] L. Xu, Phys. Rev. D **88**, 084032 (2013), arXiv:1306.2683 [astro-ph.CO].
[75] Z. Sakr (2023) arXiv:2305.02863 [astro-ph.CO].
[76] `https://github.com/MinhMPA/CAMB_GammaPrime_Growth`.
[77] D. Hanson, A. Challinor, and A. Lewis, Gen. Rel. Grav. **42**, 2197 (2010), arXiv:0911.0612 [astro-ph.CO].
[78] A. Lewis and S. Bridle, Phys. Rev. D **66**, 103511 (2002), arXiv:astro-ph/0205436.
[79] A. Lewis, Phys. Rev. D **87**, 103529 (2013), arXiv:1304.4473 [astro-ph.CO].
[80] R. M. Neal, Taking bigger metropolis steps by dragging fast variables (2005), arXiv:math/0502099 [math.ST].
[81] N. Aghanim *et al.* (Planck), Astron. Astrophys. **641**, A1 (2020), arXiv:1807.06205 [astro-ph.CO].
[82] N. Aghanim *et al.* (Planck), Astron. Astrophys. **641**, A5 (2020), arXiv:1907.12875 [astro-ph.CO].
[83] C. L. Bennett *et al.* (WMAP), Astrophys. J. Suppl. **208**, 20 (2013), arXiv:1212.5225 [astro-ph.CO].
[84] S. K. Choi *et al.* (ACT), JCAP **12**, 045, arXiv:2007.07289 [astro-ph.CO].
[85] D. Dutcher *et al.* (SPT-3G), Phys. Rev. D **104**, 022003 (2021), arXiv:2101.01684 [astro-ph.CO].
[86] S. Alam *et al.* (eBOSS), Phys. Rev. D **103**, 083533 (2021), arXiv:2007.08991 [astro-ph.CO].
[87] A. Gelman and D. B. Rubin, Statistical Science **7**, 457 (1992).
[88] E. Calabrese, A. Slosar, A. Melchiorri, G. F. Smoot, and O. Zahn, Phys. Rev. D **77**, 123531 (2008), arXiv:0803.2309 [astro-ph].
[89] E. Di Valentino, A. Melchiorri, and J. Silk, Astrophys. J. Lett. **908**, L9 (2021), arXiv:2003.04935 [astro-ph.CO].
[90] E. Di Valentino, A. Melchiorri, and J. Silk, Nature Astron. **4**, 196 (2019), arXiv:1911.02087 [astro-ph.CO].
[91] W. Handley, Phys. Rev. D **103**, L041301 (2021), arXiv:1908.09139 [astro-ph.CO].
[92] N. Aghanim *et al.* (Planck), Astron. Astrophys. **641**, A8 (2020), arXiv:1807.06210 [astro-ph.CO].

Appendix A: CMB observables in `MGCAMB` and `CAMB_GammaPrime_Growth`

In this appendix, we provide a direct comparison between the CMB observables as produced by the two codes: `MGCAMB` and `CAMB_GammaPrime_Growth`. Our aim is to understand the difference between their CMB predictions, which in turn drives the difference in their constraints on γ_L. We therefore examine a) the primary, i.e. unlensed, CMB temperature-temperature (TT) angular power spectrum $C_\ell^{\rm TT}$ and b) the CMB lensing potential angular power spectrum $C_\ell^{\phi\phi}$. We focus on the Planck(+lensing) dataset(s) and likelihood(s) as our case study. Unless explicitly stated otherwise, we adopt the best-fit base-ΛCDM cosmology in [34], specifically the "`Plik` best fit" column in their Table 1, for the following comparison.

Let us first investigate the *unlensed* CMB TT angular power spectrum as an example of primary CMB observables in the two codes. As discussed in Sec. III, with `MGCAMB`, changes in γ_L do imply changes in primary CMB observables. Specifically, the variation is significant in the lowℓ regime, as shown in Fig. 5. On the other hand, with `CAMB_GammaPrime_Growth`, no change in γ_L would alter the primary CMB observables, including the TT angular power spectrum. This is illustrated in Fig. 6.

Next, we look at the CMB lensing potentials, which should be sensitive to variations of γ_L in both codes. Comparing Fig. 7–8 and the Planck 2018 CMB lensing potential angular power spectrum [92], it is evident why `MGCAMB` prefers $\gamma_L = 0.506$ while `CAMB_GammaPrime_Growth` prefers $\gamma_L = 0.669$. Both preferences are driven by the fit to the estimated $C_\ell^{\phi\phi}$. Upon further investigation with `MGCAMB` authors[2], we have isolated and attributed the anomalous low-ℓ behavior in $C_\ell^{\phi\phi}$ from `MGCAMB` to a spurious early integrated Sachs-Wolfe (ISW) contribution from a term that contains a time-derivative instance of the modified-gravity parameter μ, i.e. $\dot{\mu}$. As pointed out and discussed in the main text, around Eq. (6), and in this appendix, this early ISW contribution significantly alters the CMB power spectra on super-horizon scales. That, in turn, shifts the data preference for γ_L. As this feature was only discovered recently, we caution the community to use `MGCAMB` with the γ_L parameterization until a fix is released. We note that other modified-gravity parameterizations in `MGCAMB`, which in fact are what `MGCAMB` was originally intended for and recommended by `MGCAMB` authors themselves[3], are still self-consistent and should be employed instead.

Finally, we have verified that adopting either best-fit cosmologies obtained by `MGCAMB` or `CAMB_GammaPrime_Growth` with "Planck+lensing" data sets (instead of "Plik best fit") does not affect our

[2] Private communication.
[3] Private communication.

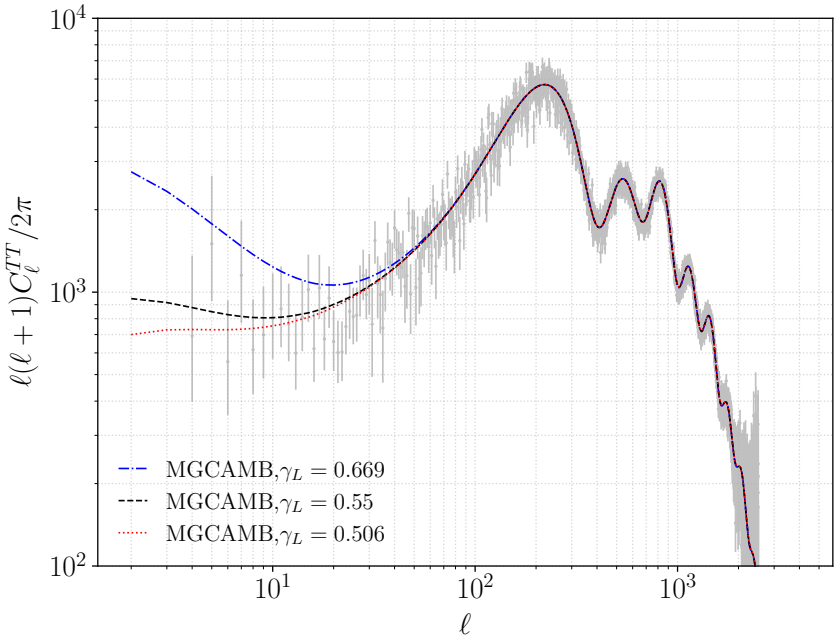


FIG. 5. The *unlensed* CMB TT angular power spectrum as predicted by `MGCAMB` at the same best-fit Planck 2018 cosmology, but for different values of γ_L. Blue and red lines correspond to the cases of $\gamma_L = 0.669$ and $\gamma_L = 0.506$ – the mean of γ_L constraints reported in the "Planck+lensing" columns in Table IV and Table VII – respectively. The black line denotes the GR case of $\gamma_L = 0.550$. The Planck 2018 measurements and their associated uncertainties are shown as grey points with error bars.

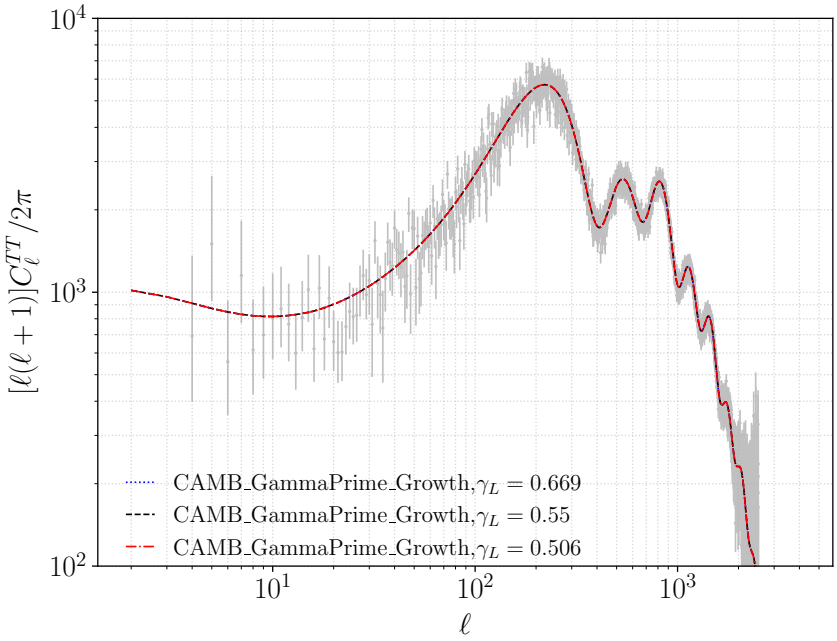


FIG. 6. Same as Fig. 5, but using `CAMB_GammaPrime_Growth`.

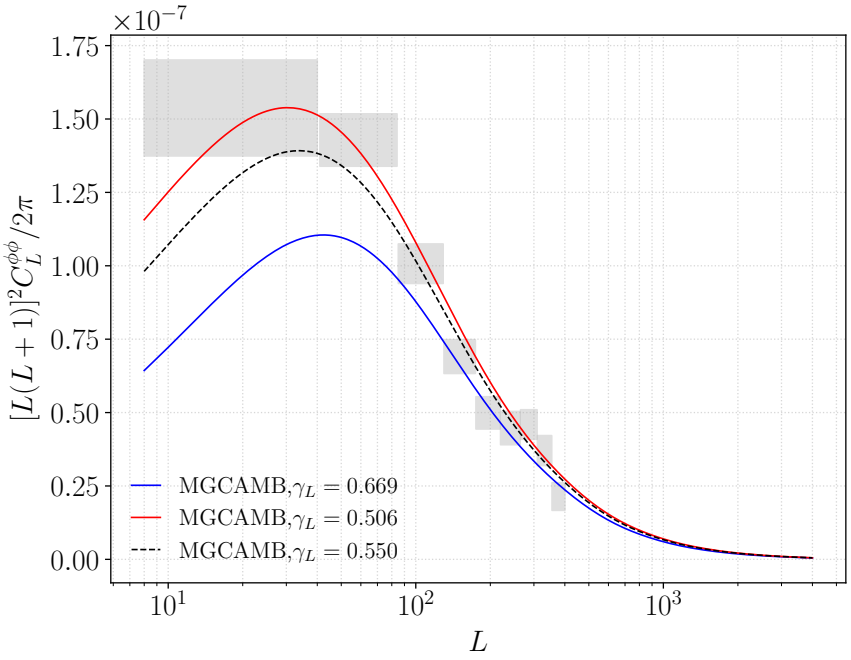


FIG. 7. The CMB lensing potential angular power spectrum as predicted by `MGCAMB` at the same best-fit Planck 2018 cosmology, for the same values of γ_L in Fig. 5–6 (following the same color notation). The Planck 2018 minimum-variance (conservative) estimates of the CMB lensing potential bandpowers and their associated uncertainties are shown as grey boxes.

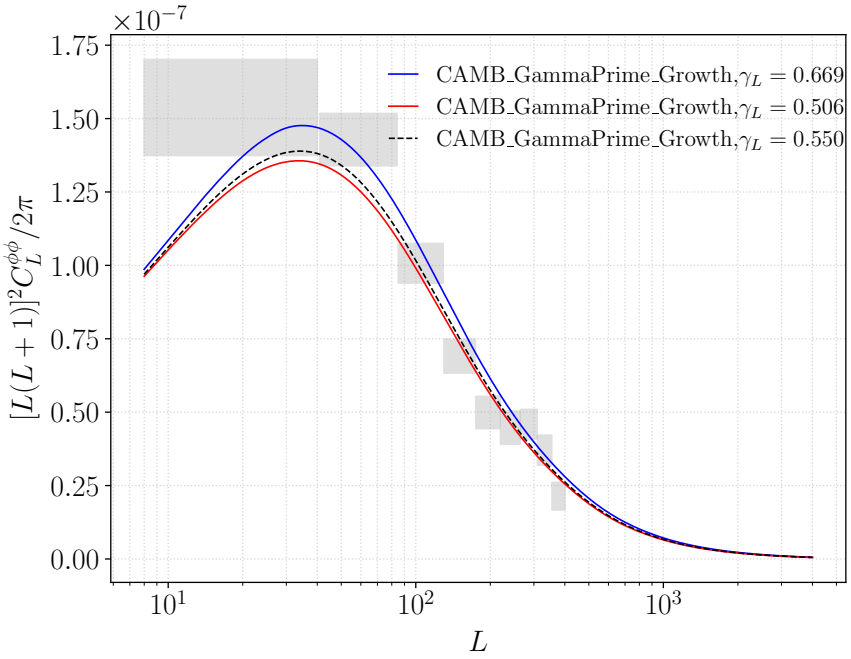


FIG. 8. Same as Fig. 5, but using `CAMB_GammaPrime_Growth`. As explained in Sec. III, with `CAMB_GammaPrime_Growth`, no change in γ_L would alter the primary CMB observables, including the TT angular power spectrum.

conclusions from this comparison.